processes

MDPI

Article

Biogenic Synthesis of Antibacterial, Hemocompatible, and Antiplatelets Lysozyme Functionalized Silver Nanoparticles through the One-Step Process for Therapeutic Applications

Pravin Dudhagara [1], Jemisha Alagiya [1], Chintan Bhagat [1], Dushyant Dudhagara [2], Anjana Ghelani [3], Jigna Desai [1], Rajesh Patel [1], Ashaka Vansia [1], Dao Ngoc Nhiem [4], Yih-Yuan Chen [5] and Douglas J. H. Shyu [6,*]

1 Department of Biosciences (UGC-SAP-II and DST-FIST-I), Veer Narmad South Gujarat University, Surat 395 007, Gujarat, India; dudhagarapr@gmail.com (P.D.); jemmy3796@gmail.com (J.A.); cbb.chintan@gmail.com (C.B.); drjigna.desai99@gmail.com (J.D.); raj252000@gmail.com (R.P.); ashaka93@gmail.com (A.V.)
2 Department of Life Sciences, Bhakta Kavi Narsinh Mehta University, Junagadh 362 263, Gujarat, India; dushyant.373@gmail.com
3 Shree Ramkrishna Institute of Computer Education and Applied Sciences, Surat 395 001, Gujarat, India; ghelanianjana@gmail.com
4 Institute of Material Science, Vietnam Academy of Science and Technology, HàNội 100000, Vietnam; nhiemdn@gmail.com
5 Department of Biochemical Science and Technology, National Chiayi University, Chiayi City 600, Taiwan; yychen@mail.ncyu.edu.tw
6 Department of Biological Science and Technology, National Pingtung University of Science and Technology, Neipu, Pingtung 912, Taiwan
* Correspondence: dshyu@mail.npust.edu.tw; Tel.: +886-8-7703202 (ext. 6367)

Abstract: To evaluate silver nanoparticles' (AgNPs) therapeutic and clinical potentials, antibacterial action, blood compatibility, and antiplatelet activities are the main concerns for toxicity profiling. Heat-denatured lysozyme-mediated formulation stabilized the AgNPs, thereby providing more bactericidal activity and blood compatibility. The study of the synthesis of AgNPs suggests the rapid and cost-effective formulation of AgNPs by one-step reaction using a 10:1 ratio of silver nitrate and lysozyme by incubating at 60 °C for two hours. Characterization of AgNPs was analyzed by UV–Visible spectroscopy, DLS, TEM, EDX, XRD, AFM, and FTIR, followed by antibacterial, hemocompatibility, and platelet aggregation testing. The average size of synthesized AgNPs was found to be 94.10 nm with 0.45 mV zeta potential and 0.293 polydispersity index by DLS. The TEM and EXD results indicated homogeneously 28.08 nm spherical-shaped pure formations of AgNPs. The XRD peaks showed the synthesis of small AgNPs with a crystallite size of 22.88 nm, while the AFM confirmed the homogeneity and smoothness of the monodispersed AgNPs. The FTIR spectra specified the coating of the lysozyme-derived amide group on the AgNPs surface, which provides stability and functionality of nanoparticles. The antibacterial activity of AgNPs was remarkable against six pathogenic bacteria and three multidrug resistance (MDR) strains (i.e., *Escherichia coli*, *Klebsiella aerogenes*, and *Pseudomonas aeruginosa*), which exhibited inhibition zones with diameters ranging between 13.5 ± 0.2 mm to 19.0 ± 0.3 mm. The non-hemolytic nature of the AgNPs was calculated by percentage hemolysis with four concentrations. The negative result of platelet aggregation using platelet-rich plasma suggests the antiplatelet effect of AgNPs. Only minor hemolysis of 6.17% in human erythrocytes and mild platelet aggregation of 1.98% were induced, respectively, by the use of 1000 µL of 1 mM AgNPs, which contains approximately 107.8 µg silver. The results indicated that the antiplatelet potency and non-hemolytic nature with the antibacterial action of the lysozyme functionalized AgNPs have a good chance to be used to solve in-stent restenosis and thrombosis issues of the coronary stent and may also have a possibility to use in vaccination to resolve the blood clotting problem. So, the optimized biogenic formulation of AgNPs offers promising opportunities to be used as a therapeutic agent.

Citation: Dudhagara, P.; Alagiya, J.; Bhagat, C.; Dudhagara, D.; Ghelani, A.; Desai, J.; Patel, R.; Vansia, A.; Nhiem, D.N.; Chen, Y.-Y.; et al. Biogenic Synthesis of Antibacterial, Hemocompatible, and Antiplatelets Lysozyme Functionalized Silver Nanoparticles through the One-Step Process for Therapeutic Applications. *Processes* **2022**, *10*, 623. https://doi.org/10.3390/pr10040623

Academic Editor: Anil K. Bhowmick

Received: 21 February 2022
Accepted: 21 March 2022
Published: 23 March 2022

Keywords: silver nanoparticles; lysozyme; antibacterial activity; hemocompatible; platelet aggregation; therapeutics

1. Introduction

Nanoparticles with less toxicity and more efficacies are indispensable materials in medicine and pharmaceutical applications. Various nanoparticles are now introduced to diagnose disease and as a therapeutic agent in the medical field. Silver nanoparticles (AgNPs) are attractive nanomaterials among several other metallic nanoparticles explored in medical science worldwide [1]. AgNPs are also well-explored for consumer product formulation and have the highest commercial application [2–4] due to their unique physicochemical and biological properties [5,6]. However, formulation methods have determined the efficacy and stability of AgNPs.

The formulation of broad-spectrum antimicrobial efficacy of biogenic colloidal AgNPs is an ongoing demand after pandemic throughout the world [7]. Conventional synthesis of AgNPs is a costly and hazardous affair requiring harsh conditions such as heavy metals and polyphenols [8]. The green alternative to the chemical synthesis of AgNPs utilizes the living organisms such as microbes, algae, fungi, plants, and animals as well as their biomolecules (especially enzymes) for the applications. Compared to conventional AgNPs synthesis methods, the green approach has been highly explored due to less or no hazardous waste production, benign, and eco-friendly process [9,10]. Additional benefits of green nanoparticle synthesis include the safer process and relatedly pure AgNPs synthesis [11]. Nowadays, overcoming the agglomeration and aggregation of AgNPs formulated using plant extract creates the need for dispersed and stable AgNPs. In addition, biogenic synthesis routes using pure form of enzymes or biocatalysts for the preparation of single-step dispersed and stable AgNPs are also attracting attention.

The toxic effects of the AgNPs are a crucial concern before their use in medical and health-related products and processes. Due to the smaller size of the AgNPs, they are translocated into blood tissue after direct or indirect exposure. The small size makes them highly reactive with blood components and adversely affects blood cells [12]. Moreover, the biological effects induced by AgNPs in the blood are dose-dependent [13].

AgNPs are well-known for their anti-inflammatory effects and improving healing effects [14]. So, a comprehensive evaluation of AgNPs biocompatibility is needed to be measured before widespread biomedical applications. The blood cell-silver nanoparticle interaction analysis is helpful in the target drug delivery system to estimate the toxicity effects of AgNPs. The pharmacological and toxicological actions and antimicrobial effectiveness of the AgNPs depend on the functionalization and physicochemical properties [15], which differ and turn on the strategic synthesis route. In this study, the biocatalyst lysozyme was used to synthesize AgNPs. Lysozyme is a 129 amino acid residue enzyme with three phenylalanine, three tyrosine, six tryptophan, and one histidine amino acid. Depending on the pH and temperature during the lysozyme crystalline process, there are two types of crystalline structure form: (i) the orthorhombic structure form at room temperature, and (ii) the tetragonal structure below room temperature [16]. After heating, lysozyme's crystal structure changes from tetragonal to orthorhombic, possessing excellent antimicrobial properties and capable of attacking cell walls of different bacterial species [17]. It indicated that the nanomaterial prepared from the lysozyme might have excellent antimicrobial properties. Shifting in amide-I peak due to interaction of lone pair of electrons on nitrogen increases the stability of the nanoparticles formed using lysozyme. Additionally, the thermal treatment also aids in denaturation of disulfide bonds present in cysteine residues of lysozyme, exposing -SH groups resulting in increased affinity towards the AgNPs and thereby stabilizing AgNPs [18]. The nano-gel prepared using lysozyme did not show any adverse effects on RBCs, suggesting its biocompatibility, which is stable for long-term storage and useful for drug delivery [19,20].

The AgNPs act as a potent bactericidal agent, and no other metal particles are comparable with its broad-spectrum antimicrobial action. The synthesis of AgNPs using lysozyme provides synergistic effects and effectively works against drug-resistant bacteria. Moreover, the lysozyme-AgNPs are non-toxic at concentrations sufficient to inhibit microbial growth [21]. In addition to antibacterial action, non-hemolytic and antiplatelet activities of AgNPs raise the hope to be used for therapeutic purposes, specifically in coronary stents coating and viral vaccine preparations [22,23]. Due to the limited literature on the biogenic formulation of such multiple features containing AgNPs, the investigation is required to establish a safe and effective therapeutic agent.

Platelets play a crucial role in facilitating the innate immune response and homeostasis [24]. Hemolysis triggered by AgNPs results in the release of hemoglobin and other fluid contents from erythrocytes, resulting in severe consequences such as anemia, jaundice, and renal failure [25]. Similarly, lysis and loss of platelets cause thrombotic disorders. Both positive and negative effects of AgNPs on platelet aggregation have been reported; however, the small-size AgNPs showed antiplatelet activity are valuable for the therapeutic and biotechnological application [22].

Nowadays, the formulation of a non-toxic and more effective nano-silver attracts the scientific community's attention. Biogenic AgNPs were synthesized using lysozyme and optimized by changing lysozyme and silver nitrate concentration, time, and temperature in this study. Following the physicochemical characterization of AgNPs, the antibacterial activity of AgNPs was investigated against six pathogenic bacteria and three multidrug-resistant (MDR) bacterial species to explore its suitability as a bactericidal agent. Hemocompatibility and platelet aggregation were investigated to explain their possible biomedical applications.

2. Materials and Methods

2.1. Materials

Silver nitrate ($AgNO_3$), triton X-100, ethylene diamine tetra-acetic acid (EDTA), sodium citrate, adenosine triphosphate (ATP) were obtained for Sisco Research Laboratory Pvt. Ltd., Mumbai, India. Lysozyme enzyme (chicken egg white—100,000 units/mg), Muller Hilton agar media, and all antibiotics disks were obtained from HiMedia Laboratory Pvt. Ltd., Mumbai, India, and used without any additional process.

2.2. Biosynthesis of AgNPs

With the 10:1 ratio of $AgNO_3$ and lysozyme, 16 reactions were prepared using four concentrations (0.1, 0.5, 1, and 2 mM) of $AgNO_3$ and four concentrations (200, 300, 400, and 500 µL) of 1 mg/mL lysozyme in 0.1 M NaOH. All reactions were incubated at 37, 60, 80, and 90 °C temperatures up to 8 h. The pH of the reaction was adjusted to 7.2 ± 0.2. The color change was observed to demonstrate the reduction of silver ions, and the time needed to form the AgNPs was confirmed by UV-Vis spectrophotometer at every 2 h interval.

2.3. Characterization of Lysozyme Functionalized AgNPs

2.3.1. UV-Vis Spectroscopy

The AgNPs synthesis was observed by the color change of the reaction mixture caused by silver ions reduction, mediated by the lysozyme, from colorless to yellowish-orange. By scanning the absorption spectrum of the reaction mixture over the range of 200 to 800 nm wavelengths, the AgNPs formation was detected by using a dual-beam UV-Vis spectrophotometer (UV-1800, Shimadzu, Japan) at 1 nm resolution [26].

2.3.2. Dynamic Light Scattering (DLS) with Zeta Potential

Zetasizer (Nano-ZS, Malvern Instruments, Malvern, Worcestershire, UK) was used to investigate the size distribution profile of the AgNPs by using d_2H_2O water as a dispersing agent. The refractive index is 1.33, and the viscosity is 0.8872 cP. The calculation of hydrodynamic size was based on the average means value of three readings. Zeta potential-based

descriptive analysis, including stability, dispersion, aggregation, or flocculation in colloidal AgNPs, was analyzed before the advanced study [27].

2.3.3. TEM and EDX Analysis

The morphology and size of AgNPs were studied using TECNAI G2 F30X TEM equipment (FEI Corp. Hillsboro, OR, USA) at 80 kV. The 50 µL AgNPs sample was attested to carbon tape. Its photographic image was taken using TEM imaging and analysis (TIA) software and visualized using TEM to check the size, shape, and agglomeration. The lattice spacing and fine morphology analysis were carried out using high-resolution TEM micrographs, and the elementary profiling of AgNPs was performed using TEM embedded EDX [28].

2.3.4. X-ray Diffraction (XRD) Analysis

Dried AgNPs were analyzed by the X-ray diffractometer on PANalyticalX'Pert Pro (USA) under the condition of 40 kV and 30 mA current at 25 °C. Through continuous scanning with position sensitive detector (PSD) mode (PSD Length °2θ = 3.35) by Cu-Kα1 radiation, the diffraction pattern was recorded with a wavelength of 1.540 Å and the step size 0.013 in the region of 2θ from 5° to 90°. The average crystalline size (D) was calculated using Debye-Scherrer equation D = 0.9 λ/βcosθ; where D is the average crystalline size, λ is the X-ray wavelength (1.5406 Å), and β is the angular full-width at half maximum (FWHM) of the XRD peak at the diffraction angle θ [29].

2.3.5. Atomic Force Microscopy (AFM)

AFM was used to investigate the dispersion and aggregation of AgNPs. A thin film of AgNPs was deposited on a silica glass plate by drops dropping the AgNPs on the plate and allowed to dry at room temperature for 12 h in the dark and then subjected to AFM analysis (CSPM-5500, Karaltay (Beijing) Instruments Co. Ltd., Beijing, China) [30]. The diameter was estimated according to the following equation; Robs = 4 (RtRp)1/2, where Robs, Rt, and RP denote the observed particle radius, tip radius (10 nm, manufactures specification), and actual radius of the particle, respectively.

2.3.6. Fourier Transform Infrared Spectroscopy (FTIR)

The solution of AgNPs was dried at 65 °C, and the dried powders were subjected to FTIR analysis in the range of 4000–4500 cm^{-1} using the KBr pellet method to identify the active group in lysozymes involved in the formation of AgNPs. The FTIR spectra were obtained using a Spectrum Two FT-IR Spectrometer (Perkin-Elmer, Waltham, MA, USA) [31]. The spectrometer operated in the diffuse reflectance mode at a resolution of 4 cm^{-1} with a speed scan of 0.2 cm/s.

2.3.7. Antibacterial Activity

Antibacterial activity of AgNPs was performed using a well diffusion method [26] against six laboratory-isolated pathogens and three MDR strains of bacterial species. Six pathogenic bacteria, *Escherichia coli*, *Klebsiella aerogenes*, *Bacillus subtilis*, *Bacillus licheniformis*, *Pseudomonas aeruginosa*, and *Klebsiella pneumoniae*, were isolated from clinical samples provided by the Microcare laboratory, Surat, India. Three MDR bacterial species were also used to test the antimicrobial potential of AgNPs. The MDR strains of *Escherichia coli*, *Klebsiella aerogenes*, and *Pseudomonas aeruginosa* were tested using 30, 35, and 32 antibiotics, respectively (Supplementary data file Table S1 and Figures S1–S3). The antibiotic resistance profile was performed following CLSI guidelines—M100 ED 32 (2022) [32]. The sterile cotton swabs were used to evenly spread the bacterial culture onto the Muller-Hilton (MH) agar plates to investigate antibacterial efficacy. The sterilized agar cup borer was used to punch the 9 mm hole in MH agar, and 100 µL of AgNPs were added. The antibacterial activity of 100 µL of 1 mM AgNPs was measured as the size of the zone of inhibition (ZOI) in mm against the ZOI of 1 mM $AgNO_3$ solution (100 µL) to determine its efficiency. The

inhibition zone was measured after 24 h incubation at 37 °C. The sterile distilled water (100 µL) was used as the control.

2.3.8. Blood Collection

Blood was withdrawn from healthy adult volunteers who had not been on any medication known to interfere with RBC and platelet function for at least one month before the study. The medical officer did collection as per the institutional policy of the blood-bank (Surat Rakdan Kendra). Blood was collected in EDTA vials for in vitro hemolytic activity. Blood was collected in the vial containing 3.2% sodium citrate for the platelet aggregation activity.

2.3.9. Hemolytic Activity

The test described by Huang et al. [13] was performed in triplicate by the spectrophotometric method of hemoglobin released after exposure to different concentrations of AgNPs. Whole blood was collected in an EDTA vial, and its total blood hemoglobin (TBH) was adjusted to a concentration of 10 mg/mL by the addition of normal saline. Normal saline and 1% Triton X-100 were negative and positive controls, respectively. The mixture was incubated at 37 °C for three hours. Then, the samples were centrifuged at 800× *g* for 15 min. The absorbance of the supernatant was measured at 450 nm. The reaction mixture was prepared using four volumes of 1 mM AgNPs (Table 1). The percentage of hemolysis was calculated from the following formula. The significance threshold was set at 0.05.

$$\% \text{ Hemolysis} = \frac{(\text{absorbance of sample}) - (\text{absorbance of negative control})}{(\text{absorbance of posi ive control} - \text{absorbance of negative control})} \quad (1)$$

Table 1. Hemolytic activity of the AgNPs using healthy volunteer blood.

Reaction Tube	Dilute Human Blood	1%Triton X-100	Normal Saline	1 mM AgNPs
Positive Control	100 µL	100 µL	Not Added	Not Added
Negative Control	100 µL	Not Added	100 µL	Not Added
Test-1	100 µL	Not Added	Not Added	1000 µL
Test-2	100 µL	Not Added	Not Added	500 µL
Test-3	100 µL	Not Added	Not Added	250 µL
Test-4	100 µL	Not Added	Not Added	100 µL

2.3.10. Platelet Aggregation Activity

Platelet-rich plasma (PRP) was obtained from the blood collected in sodium citrate-containing vial by centrifugation at 110× *g* for 10 min at room temperature [33]. The collected supernatant was diluted with Tyrode's solution containing bovine serum albumin (3.5 mg/mL). Adenosine triphosphate (ATP) and crude potato extract as a source of apyrase [34] were used as a positive control, and normal saline was used as a negative control. The reaction mixture with two tests was prepared, as shown in Table 2. The test reaction mixture was incubated at 37 °C for 15 min, followed by making up the final volume of 1000 µL with normal saline. The absorbance was measured at 415 nm, and the percentage of platelet aggregation as inhibition (PI) was calculated from the formula shown below. The reactions were performed in triplicates.

$$\text{PI } (\%) = \frac{(\text{A} - \text{B})}{\text{A}} \times 100 \quad (2)$$

where PI = Percentage of Aggregation, A = Absorbance of Blank, B = Absorbance of Test.

Table 2. Platelet aggregation of AgNPs using platelet-rich plasma.

Reaction Tube	Platelet-Rich Plasma (PRP)	ATP	Apyrase (Potato Extract)	Normal Saline	1 mM AgNPs
Positive Control	500 µL	5 µM	10 µL	Not Added	Not Added
Negative Control	500 µL	Not Added	Not Added	500 µL	Not Added
Test-1	500 µL	Not Added	Not Added	Not Added	500 µL
Test-2	1000 µL	Not Added	Not Added	Not Added	1000 µL

2.3.11. Statistical Analysis

The data obtained were presented as mean ± standard error of the mean (SEM) and plotted with Microsoft Excel. One-way analysis of variance (ANOVA) was used to examine the significant difference between groups and * indicates $p < 0.05$ between groups.

3. Result and Discussion

3.1. Synthesis of AgNPs and Spectroscopic Analysis

From all reactions using different concentrations of $AgNO_3$ and lysozyme, the optimized synthesis of homogenous and stable AgNPs was observed with one mM $AgNO_3$, 200 µg of lysozyme at 60 °C after two h of incubation. The result of UV-Vis spectroscopic analysis showed the narrow bell-shaped curve, and the highest absorbance was recorded at 425 nm to confirm the formation of homogenous AgNPs. The reduction of the silver ions was increased as the time, and temperature increased, leading to the color changes from colorless to yellow and finally orange in all reaction mixtures, which indicates the growth of AgNPs (Figure 1). The AgNPs synthesis was found to be time and temperature-dependent. Due to the thiol group in the enzyme's active site being sensitive and reactive with silver ions [5,35], high temperature and prolonged time provide better accessibility of silver ions to interact with thiol groups of the unfolded enzyme leading to the quick reduction of silver to form nano-silver [36]. The results indicated that 60 °C temperature for two h was the optimum condition to develop homogeneous and monodispersed AgNPs. It showed that the synthesis rate could be facilitated by increasing the reaction time and temperature [37]. However, temperatures above 60 °C broadened the peak. It is suggested that the formation of bigger and less monodisperse particles may be led to the absorption decrease due to the denaturation of the enzyme at higher temperatures [38].

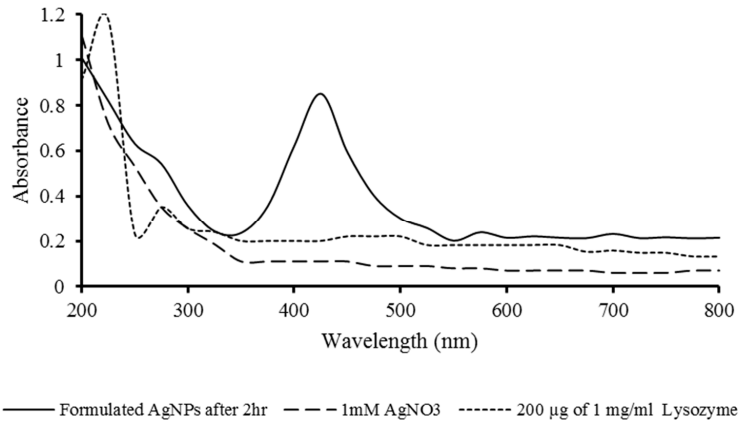

Figure 1. The UV-Visible spectrum of AgNPs was synthesized using a 10:1 ratio of 1 mM silver nitrate and 200 µL lysozyme (1 mg/mL) after 2 h incubation at 60 °C along with UV-visible spectra of a 1 mM $AgNO_3$ and 1 mg/mL of 200 µL lysozyme.

The nucleation step of the silver ions is the critical process for the growth of nanoparticles to determine their sizes. The amino and carboxyl groups and other functional groups (i.e., hydroxyl and phenoxy groups) of an enzyme are involved in the nucleation step

for the biosynthesis of nanoparticles [39,40]. Lysozyme is rich in aromatic amino acids, such as tryptophan and tyrosine and the phenoxy group of tyrosine, and are well-known moieties for interaction with silver [41]. The active functional moieties of the lysozyme are suggested to be responsible for the nucleation of the silver ions and the growth of AgNPs by a bottom-up approach. Similar studies were performed for silver nanoparticle synthesis using lysozyme and borohydramide reduction method [18,42,43]. Here, an alternative method with ATP and EDTA was used for nanoparticle synthesis in addition to chicken lysozyme.

3.2. Particle Size, Charge, and Polydispersity

The size distribution profile of AgNPs showed an average size of 94.10 nm by intensity, number with polydispersity index 0.293, and zeta potential value is 0.45 mV (Figure 2). This finding is similar to the earlier report of the biogenic synthesis of AgNPs by *Pseudomonas* sp. [44]. The lower value of the polydispersity index indicates the stable and controlled quality of the nanoparticles, which is essential for the nanocarrier formulations in clinical and therapeutic applications [45]. The positive value of zeta potential indicates a quantitative value for the overall surface charge of the AgNPs. Furthermore, it is also an indication to show the colloidal stability of the nano-silver. The higher absolute zeta potential also indicates the greater electrostatic repulsion between nanoparticles. Hence, the colloidal AgNPs are more stable with less incidence of agglomeration. The size distribution profile of AgNPs showed an average size of 94.10 nm by intensity, number with polydispersity index 0.293, and zeta potential value is 0.45 mV (Figure 2). This finding is similar to the earlier report of the biogenic synthesis of AgNPs by *Pseudomonas* sp. [44]. The lower value of the polydispersity index indicates the stable and controlled quality of the nanoparticles, which is essential for the nanocarrier formulations in clinical and therapeutic applications [45]. The positive value of zeta potential indicates a quantitative value for the overall surface charge of the AgNPs.

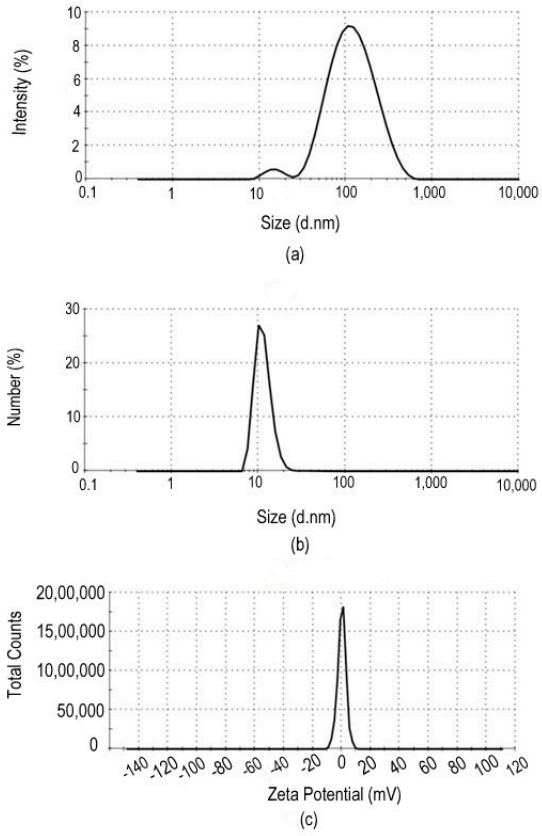

Figure 2. Particle size distribution of AgNPs with respect to (**a**) intensity, (**b**) number, and (**c**) Zeta Potential 0.45 (mV).

Furthermore, it is also an indication to show the colloidal stability of the nano-silver. The higher absolute zeta potential is an indication of the greater electrostatic repulsion between nanoparticles. Hence, the colloidal AgNPs are more stable with less incidence of agglomeration.

3.3. TEM and EDX Analysis

The results of the scattered particles in TEM analysis divulged the spherical shape of AgNPs with an average diameter of 28.08 nm. The homogeneous small size of AgNPs was further analyzed using high-resolution TEM (HRTEM), and the perfect atomic arrangement was reported. The HRTEM image of AgNPs shows clear lattice fringes arranged due to (111) planes, which can be indexed with a face-centered cubic with a spacing of 0.23 nm. Energy-dispersive X-ray spectra of AgNPs showed the clear and sharp peak of metallic silver nanocrystals at 3 keV, confirming the presence of elemental silver, which is due to the surface plasmon resonance of AgNPs (Figure 3). The EDX result agreed with earlier biogenic AgNPs formulation [46]. The high purity of the formulated AgNPs is suggestive of the impending application in the biomedical field.

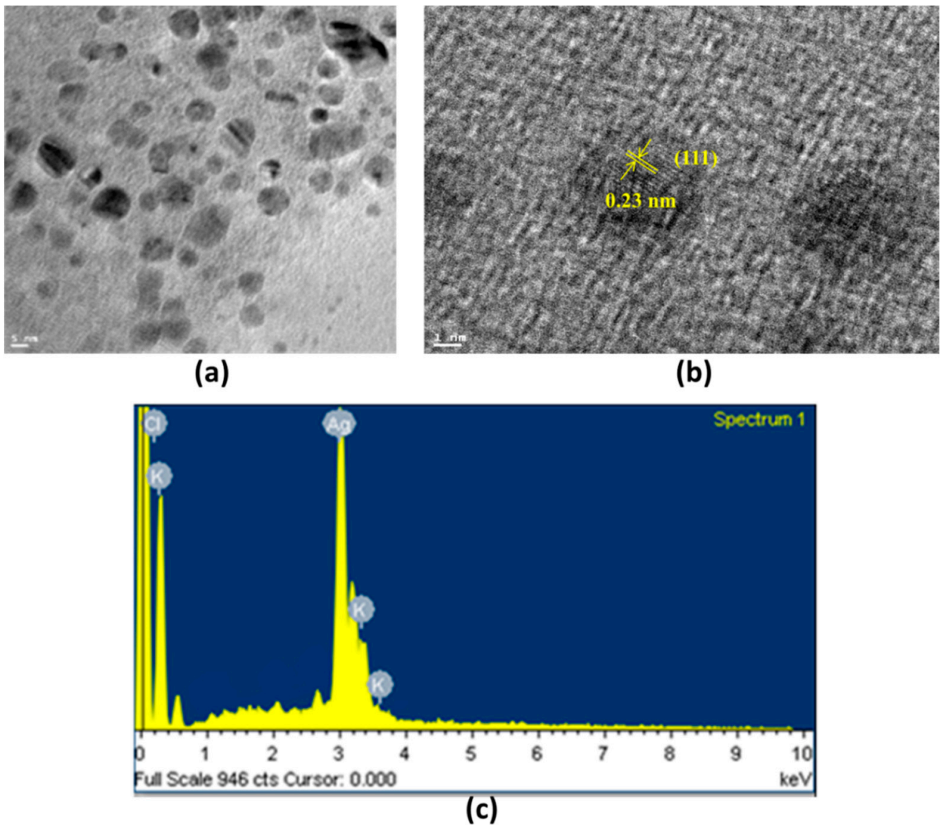

Figure 3. (**a**) TEM analysis of AgNPs indicating the scattered and spherical shapes with an average size of 28.08 nm (Scale bar: 5 nm). (**b**) HRTEM image at 1 nm (100 Å) indicates crystalline formation arrangement in AgNPs. (The lattice spacing 0.23 nm of AgNP (111) plane in high-resolution TEM image). (**c**) Elemental profiling using EDX spectra.

3.4. XRD Analysis

XRD analysis confirmed the presence of four distinct diffraction peaks at 38.31°, 44.48°, 64.61°, and 77.51°, which indexed the planes of (111), (200), (220), and (311), respectively. XRD analysis showed that the AgNPs conform to a face-centered cubic crystalline phase. Due to the biogenic route of synthesis, a few minor unassigned peaks were also observed (Figure 4). The broadening of the Bragg's peaks around their bases shows the formation of small-sized AgNPs [47]. Using the standard Debye- Scherrer method, the average crystallite size (grain) was found at 22.88 nm (Table 3).

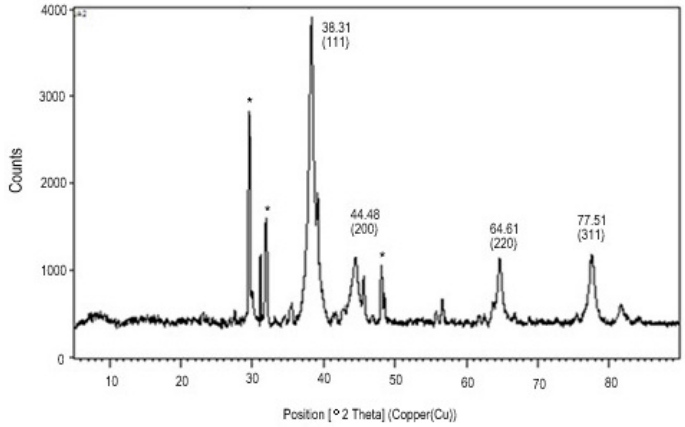

Figure 4. XRD pattern of AgNP displaying peak indices and 2θ positions. (* shows the extra unassigned peaks of enzyme and its peptide).

Table 3. Crystallite (Grain) size of AgNPs calculated using Debye–Scherrer's equation using XRD data.

Peak Position (2θ)	Planes-hkl	FWHM (2θ)	Crystallite Size (nm)	Average Crystalline Size (nm)
38.3182	111	0.3814	23.01	22.88
44.4893	200	0.5828	15.37	
64.6176	220	0.3458	28.37	
77.5102	311	0.4293	24.77	

3.5. AFM Analysis

The AFM tip analyses the surface of nanoparticles and records their topography to elucidate the shape, size, and surface of nanoparticles after desiccating the samples. 2D horizontal cross-section of AFM analysis revealed monodispersed and spherical AgNPs. A three-dimensional image of AFM showed the average smoothness and homogeneity of AgNPs (Figure 5). The absence of agglomeration with an average size of 60 nm indicates the possibility to store AgNPs for the long term before actual use in clinical and biomedical applications.

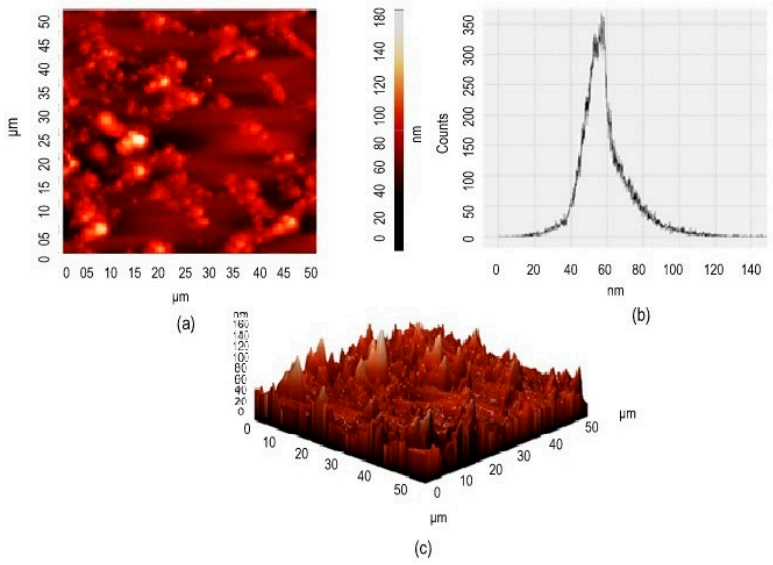

Figure 5. AFM analysis of silver nanoparticles: (**a**) 2D image of AgNPs horizontal cross-section; (**b**) histogram showing average particle size; (**c**) 3D image of AgNPs.

3.6. FTIR Spectroscopy

FTIR spectra are valuable for monitoring the secondary structural property of proteins [48] and are thus helpful to characterize enzyme-coated metal nanoparticles. FTIR measurements were performed to identify the presence of the surface charge and functional group in the lysozyme functionalized AgNPs. The IR analysis revealed the strong and sharp band peaks at 3350.14, 2127.89, and 1638.63 cm^{-1} were assigned to the stretching vibrations of amide III (O-H stretch), amide II (C-H stretch), and amide I (C=O stretch), respectively (Figure 6). The band frequencies can be easily correlated with the protein structure, indicating the capping of AgNPs with amines bonding of lysozyme. The capping with enzyme-derived amines is responsible for the overall stability of AgNPs.

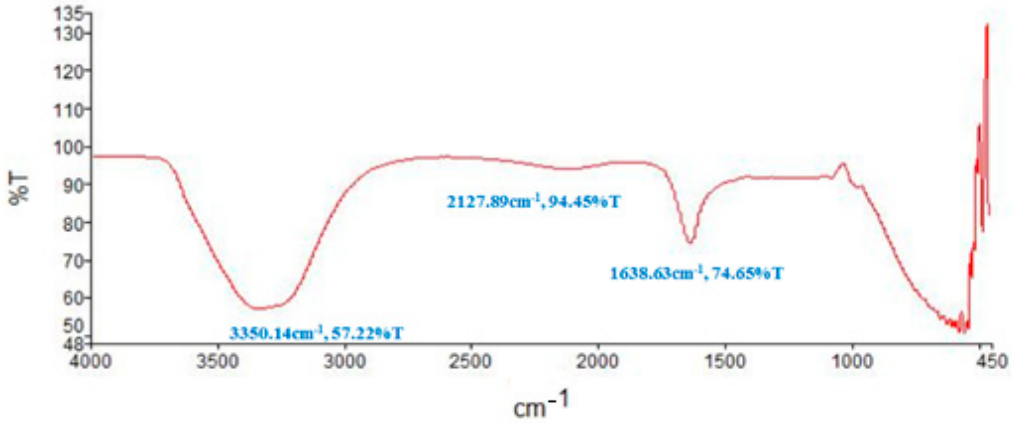

Figure 6. FTIR spectra of lysozyme functionalized AgNPs.

3.7. Antimicrobial Activity

Antimicrobial resistance (AMR) of pathogenic microbes and infection control are global issues of great challenge. Various potential antimicrobial drugs have been tried to treat the infections from AMR bacteria, and the search for new antimicrobial substances against MDR species is ongoing. Due to the various antimicrobial mechanisms of AgNPs, it could be one of the best solutions to solve the resistant problems of bacteria [49,50]. In this study, the highest antibacterial activity of AgNPs was observed against Klebsiella pneumoniae, followed by *Escherichia coli*, *Klebsiella aerogenes*, Bacillus licheniformis, Bacillus subtilis, and the lowest antibacterial activity of AgNPs was observed against *Pseudomonas aeruginosa*. Furthermore, the results of the antimicrobial activity of AgNPs against three pathogenic MDR strains of *Escherichia coli*, *Klebsiella aerogenes*, and *Pseudomonas aeruginosa* exhibited inhibition zones with diameters ranging between 13.5 ± 0.2 mm to 19.0 ± 0.3 mm, which is far better than $AgNO_3$ (Table 4). The AgNPs demonstrated powerful bactericidal effects on all gram-negative non-MDR and MDR bacteria (Supplementary data). The AgNPs interact with enzymes and proteins, modify the cell wall structure, alter membrane permeability, and inhibit respiratory activity leading to the death of the bacteria [51]. AgNPs are easily diffused across the membrane of Gram-negative bacteria due to the negative electrostatic charges present in their membranes. The membrane allows the entry of smaller AgNPs inside the cell. The smaller the size of the AgNPs make them easier to penetrate the bacterial cells [36,52].

Furthermore, smaller AgNPs are destructive against bacterial cell membrane and cell wall by forming free radicals to induce the release of reactive oxygen species (ROS) such as H_2O_2, O_2^-, OH^-, O_2^{*-} etc. with decisive bactericidal action. However, it is still a matter of debate, but the involvement of AgNPs mediated ROS is well reported in cell destruction [53–55]. However, the variation of AgNPs' response to different bacterial species is due to bacteria's metabolic diversity and inherent characteristics [56]. Hence, *Pseudomonas aeruginosa* was reported more resistant than *E. coli*. Also, the result of effective antibacterial activity against MDR strain indicates the role of lysozyme as a coating agent.

Table 4. Antibacterial activity of colloidal 1mM AgNPs against laboratory pathogens and MDR strains.

Laboratory Isolated Bacterial Species	ZOI of 100 µL $AgNO_3$ (mm)	ZOI of 100 µL AgNPs (mm)	ZOI 100 µL Distilled Water (mm)
Gram-positive			
Bacillus licheniformis	10.0 ± 0.6	14.5 ± 0.7	0.0
Bacillus subtilis	12.5 ± 0.4	14.5 ± 0.8	0.0
Gram-negative			
Escherichia coli	14.0 ± 0.5	19.0 ± 0.3	0.0
Klebsiella aerogenes	12.0 ± 0.8	15.0 ± 0.6	0.0
Klebsiella pneumoniae	16.0 ± 0.2	20.0 ± 0.6	0.0
Pseudomonas aeruginosa	10.0 ± 0.6	14.0 ± 0.5	0.0
Escherichia coli (MDR) *	15.0 ± 0.3	19.0 ± 0.3	0.0
Klebsiella aerogenes (MDR) *	15.0 ± 0.4	17.5 ± 0.5	0.0
Pseudomonas aeruginosa (MDR) *	11.0 ± 0.2	13.5 ± 0.2	0.0

ZOI, zone of inhibition; Multidrug resistance has been checked according to the Clinical and Laboratory Standards Institute (CLSI) standards 2022 [32]. Available online: https://clsi.org/ (accessed on 18 March 2022). * All three MDR were extended spectrum beta-lactamase (ESBL) and metallo beta-lactamase (MBL) positive strains evaluated by the E-test (Supplementary Figure S4). The E-test strips were purchased from HiMedia Laboratories Pvt Ltd., Mumbai, India.

3.8. Hemolytic Activity

To analyze the hemolysis, 100, 250, and 500 µL of 1 mM AgNPs were found non-hemolytic after three repetitive reactions. However, 1000 µL of 1 mM AgNPs (contains approx. 107.8 µg silver) could induce minor hemolysis (6.17%) in human erythrocytes (Figure 7). The AgNPs mediated hemolysis is size and dose-dependent process. Small size (15 nm) AgNPs have the highest tendency to induce hemolysis compared to bigger a size (50 to 100 nm) of AgNPs [57]. In addition, the capping agents and coating medium of AgNPs play important roles in the hemolysis of human erythrocytes. The result suggests that lysozyme-coated AgNPs are suitable for intravenous or subtropical applications. Our result is better than the earlier reported 19% hemolysis by approximately 40 µg/mL of polyvinylpyrrolidone-coated AgNPs with a size of 21.6 ± 4.8 nm [13]. However, it remains difficult to compare results of AgNPs-triggered hemolysis across different studies due to the lack of physicochemical characterization and in vitro hemolysis standards. Nevertheless, our results are in good agreement with previous reports [57,58]. Usually, in the hemolysis process, the AgNPs interact with RBC in vitro and cause ROS production. The AgNPs may also alter the membrane of erythrocytes, causing pores and leading to osmotic lysis [58]. However, the exact reason for AgNPs-induced hemolysis has not yet been clearly demonstrated, and many more mechanisms might contribute to hemolysis, including deformability, adhesiveness, and membrane vesiculation of RBCs.

3.9. Platelet Aggregation Activity

Platelet aggregation (0.19%) was not observed in the presence of 500 µL of 1 mM AgNPs (containing approx. 53.9 µg silver), suggesting the antiplatelet effect of AgNPs. The mild aggregation (1.98%) was found in the presence of 1000 µL of 1mM AgNPs (contains approx. 107.8 µg silver) (Figure 8). The in vitro blood compatibility study of AgNPs is a controversial topic due to morphologically different AgNPs reacting with platelet differentially (i.e., either no impact or platelet aggregation). In addition to the morphological features of AgNPs, coating agents also play essential roles in the aggregation of platelets [59]. As a natural molecule of the immune system, lysozyme does not induce adverse effects such as inflammation or other clinical ailments. The antiplatelet properties may be due to the coating of lysozyme on AgNPs. However, the current result is qualitative

only. More experimental works should be executed to confirm the reason for the antiplatelet activity of AgNPs.

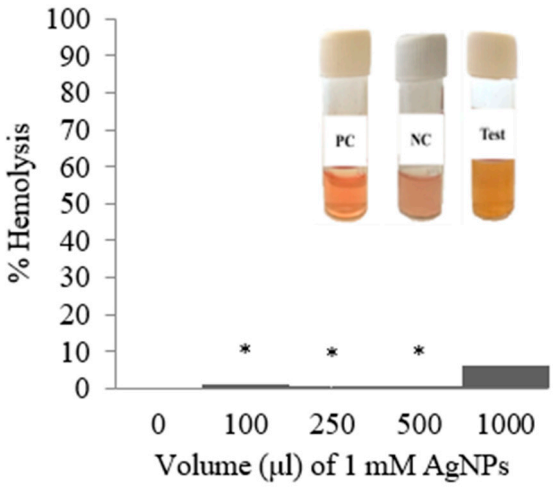

Figure 7. Hemolysis of human erythrocyte at the different volumes of 1 mM AgNPs. A satellite image shows reaction tubes after 3 h incubation at 37 °C temperature. (PC, positive control; NC, negative control; Test, 1000 µL of 1 mM AgNPs, and * $p < 0.05$).

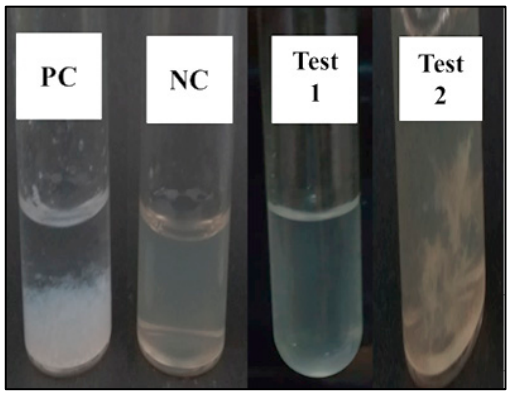

Figure 8. Platelets aggregation of AgNPs (PC, positive control; NC, negative control; Test1, 500 µL of AgNPs; Test 2, 1000 µL of AgNPs).

The key factors responsible for the antiplatelet activity of silver include AgNPs size, shape, surface charge, coating agents, and impurities. Similarly, platelet biological features are also responsible, including the physiological state of platelets before the exposure of AgNPs [51,60,61]. Furthermore, proper methods are also required to detect mild aggregation and micro-aggregation of platelets.

The antibacterial, non-hemolytic, and antiplatelet nature has specified the possibilities to prepare safe and effective AgNPs-coated coronary stents. They may be used as potent molecules to reduce blood clotting, such as the adverse effects of the COVID-19 vaccine in a vaccinated person. However, this study provides only baseline information of AgNPs formulation, characteristics, and therapeutic applicability. The side effects of AgNPs and cytotoxicity in human cells must be investigated to establish the AgNPs as a safe therapeutic agent.

4. Conclusions

Single-step synthesis of functionalized, non-toxic, and more effective silver nanoparticles has been produced using lysozyme as a reducing agent. In addition, the lysozyme-AgNP conjugate was proved to achieve a synergic antibacterial effect since heat-denatured lysozyme-stabilized silver nanoparticles are more bactericidal [62]. AgNPs synthesis using

a 10:1 ratio of 1 mM $AgNO_3$ and 1 mg/mL of lysozyme at 60 °C for 120 min incubation is a viable and scalable process at the large-scale synthesis. Lysozyme-mediated silver ions reduction stabilized the AgNPs and assisted in the ripening of the nanoparticles. In narrow bell-shaped graphs, the synthesized AgNPs showed the SPR peak at 425 nm. The spherical, monodispersed, and mild positive surface charge containing AgNPs was found stable and free from impurities, revealing the suitability for therapeutic and clinical uses. Formulating controlled-size and scattered AgNPs with crystalline nature is suitable for biotechnological applications. The amide functional groups on the AgNPs make them reactive with remarkable antibacterial activity against non-MDR and MDR strains of pathogenic bacteria. The lysozyme-coated AgNPs exhibited non-hemolytic activity and antiplatelet effects. The results indicate that the physicochemical and biological characteristics of lysozyme functionalized AgNPs are significant for the impending application as nanotherapeutics and nanomedicine.

Supplementary Materials: The following are available online at https://www.mdpi.com/article/10.3390/pr10040623/s1. Table S1: Antibiotics susceptibility test to evaluate the MDR profile of *E. coli*, *K. aerogenes*, and *P. aeruginosa*; Figure S1: Images of antimicrobial susceptibility test performed to evaluate the MDR profile of *E. coli*; Figure S2: Images of antimicrobial susceptibility test performed to evaluate the MDR profile of *K. aerogenes*; Figure S3: Images of antimicrobial susceptibility test performed to evaluate the MDR profile of *P. aeruginosa*; Figure S4: The E-test performed to evaluate the MDR profile of (**A**) *P. aeruginosa*, (**B**) *K. aerogenes*, and (**C**) *E. coli*. All strains are extended spectrum beta-lactamase (ESBL) and metallo beta-lactamase (MBL).

Author Contributions: Conceptualization, P.D., J.A. and C.B.; methodology, D.D. and A.G.; writing—original draft preparation, J.D., R.P., A.V. and D.N.N.; writing—review and editing, Y.-Y.C. and D.J.H.S.; supervision, P.D. and D.J.H.S.; project administration, P.D. and J.A. All authors have read and agreed to the published version of the manuscript.

Funding: This research received no external funding.

Institutional Review Board Statement: The study was conducted in accordance with the Declaration of Helsinki. Ethical review and approval were waived for this study due to the use of pre-collected and anonymized samples. Pre-collected blood was procured from blood-bank (Surat Raktdan Kendra & Research Centre, Surat, Gujarat, India) on non-profit basis.

Informed Consent Statement: Patient consent was waived due to the use of pre-collected and anonymized samples. Pre-collected blood was procured from blood-bank (Surat Raktdan Kendra & Research Centre, Surat, Gujarat, India) on non-profit basis.

Data Availability Statement: Not applicable.

Acknowledgments: The authors are thankful for providing the UGC-SAP-II and DST-FIST-I resources to initiate the experimental work. The authors are thankful to Microcare Laboratory, Surat, India (Available online: https://www.microcarelab.in/) (accessed on 18 March 2022) for providing the clinical samples for isolation of pathogenic bacterial species and evaluation of antibiotic resistance of the isolates.

Conflicts of Interest: There are no conflict of interest.

References

1. Zhang, X.-F.; Liu, Z.-G.; Shen, W.; Gurunathan, S. Silver nanoparticles: Synthesis, characterization, properties, applications, and therapeutic approaches. *Int. J. Mol. Sci.* **2016**, *17*, 1534. [CrossRef]
2. Lee, S.H.; Jun, B.-H. Silver nanoparticles: Synthesis and application for nanomedicine. *Int. J. Mol. Sci.* **2019**, *20*, 865. [CrossRef]
3. Tulve, N.S.; Stefaniak, A.B.; Vance, M.E.; Rogers, K.; Mwilu, S.; LeBouf, R.F.; Schwegler-Berry, D.; Willis, R.; Thomas, T.A.; Marr, L.C. Characterization of silver nanoparticles in selected consumer products and its relevance for predicting children's potential exposures. *Int. J. Hyg. Environ. Health* **2015**, *218*, 345–357. [CrossRef]
4. Ahamed, M.; AlSalhi, M.S.; Siddiqui, M.K.J. Silver nanoparticle applications and human health. *Clin. Chim. Acta* **2010**, *411*, 1841–1848. [CrossRef]
5. Sharma, V.K.; Yngard, R.A.; Lin, Y. Silver nanoparticles: Green synthesis and their antimicrobial activities. *Adv. Colloid Interface Sci.* **2009**, *145*, 83–96. [CrossRef] [PubMed]

6. Krutyakov, Y.A.; Kudrinskiy, A.A.; Olenin, A.Y.; Lisichkin, G.V. Synthesis and properties of silver nanoparticles: Advances and prospects. *Russ. Chem. Rev.* **2008**, *77*, 233. [CrossRef]
7. Ansari, M.A.; Kalam, A.; Al-Sehemi, A.G.; Alomary, M.N.; AlYahya, S.; Aziz, M.K.; Srivastava, S.; Alghamdi, S.; Akhtar, S.; Almalki, H.D.; et al. Counteraction of biofilm formation and antimicrobial potential of *Terminalia catappa* functionalized silver nanoparticles against *Candida albicans* and multidrug-resistant Gram-negative and Gram-positive bacteria. *Antibiotics* **2021**, *10*, 725. [CrossRef]
8. El-Seedi, H.R.; El-Shabasy, R.M.; Khalifa, S.A.M.; Saeed, A.; Shah, A.; Shah, R.; Jan Iftikhar, F.; Abdel-Daim, M.M.; Omri, A.; Hajrahand, N.H.; et al. Metal nanoparticles fabricated by green chemistry using natural extracts: Biosynthesis, mechanisms, and applications. *RSC Adv.* **2019**, *9*, 24539–24559. [CrossRef]
9. Jabir, M.S.; Saleh, Y.M.; Sulaiman, G.M.; Yaseen, N.Y.; Sahib, U.I.; Dewir, Y.H.; Alwahibi, M.S.; Soliman, D.A. Green synthesis of silver nanoparticles using *Annona muricata* extract as an inducer of apoptosis in cancer cells and inhibitor for NLRP3 inflammasome via enhanced autophagy. *Nanomaterials* **2021**, *11*, 384. [CrossRef] [PubMed]
10. Hawar, S.N.; Al-Shmgani, H.S.; Al-Kubaisi, Z.A.; Sulaiman, G.M.; Dewir, Y.H.; Rikisahedew, J.J. Green synthesis of silver nanoparticles from *Alhagi graecorum* leaf extract and evaluation of their cytotoxicity and antifungal activity. *J. Nanomater.* **2022**, *2022*, 1058119. [CrossRef]
11. Vishwanath, R.; Negi, B. Conventional and green methods of synthesis of silver nanoparticles and their antimicrobial properties. *Curr. Res. Green Sustain. Chem.* **2021**, *4*, 100205. [CrossRef]
12. Hante, N.K.; Medina, C.; Santos-Martinez, M.J. Effect on platelet function of metal-based nanoparticles developed for medical applications. *Front. Cardiovasc. Med.* **2019**, *6*, 139. [CrossRef] [PubMed]
13. Huang, H.; Lai, W.; Cui, M.; Liang, L.; Lin, Y.; Fang, Q.; Liu, Y.; Xie, L. An evaluation of blood compatibility of silver nanoparticles. *Sci. Rep.* **2016**, *6*, 25518. [CrossRef] [PubMed]
14. Kwan, K.H.; Yeung, K.W.; Liu, X.; Wong, K.K.; Shum, H.C.; Lam, Y.W.; Cheng, S.H.; Cheung, K.M.; To, M.K. Silver nano-particles alter proteoglycan expression in the promotion of tendon repair. *Nanomedicine* **2014**, *10*, 1375–1383. [CrossRef] [PubMed]
15. Petros, R.A.; DeSimone, J.M. Strategies in the design of nanoparticles for therapeutic applications. *Nat. Rev. Drug Discov.* **2010**, *9*, 615–627. [CrossRef] [PubMed]
16. Salinas-Garcia, M.C.; Plaza-Garrido, M.; Alba-Elena, D.; Camara-Artigas, A. Major conformational changes in the structure of lysozyme obtained from a crystal with a very low solvent content. *Acta Crystallogr. Sect. F Struct. Biol. Commun.* **2019**, *75*, 687–696. [CrossRef]
17. Jollès, P.; Berthou, J. High temperature crystallization of lysozyme: An example of phase transition. *FEBS Lett.* **1972**, *23*, 21–23. [CrossRef]
18. Ashraf, S.; Chatha, M.A.; Ejaz, W.; Janjua, H.A.; Hussain, I. Lysozyme-coated silver nanoparticles for differentiating bacterial strains on the basis of antibacterial activity. *Nanoscale Res. Lett.* **2014**, *9*, 565. [CrossRef]
19. Pan, D.C.; Myerson, J.W.; Brenner, J.S.; Patel, P.N.; Anselmo, A.C.; Mitragotri, S.; Muzykantov, V. Nanoparticle properties modulate their attachment and effect on carrier red blood cells. *Sci. Rep.* **2018**, *8*, 1615. [CrossRef]
20. Li, J.; Yu, S.; Yao, P.; Jiang, M. Lysozyme−dextran core-shell nanogels prepared via a green process. *Langmuir* **2008**, *24*, 3486–3492. [CrossRef]
21. Eby, D.M.; Schaeublin, N.M.; Farrington, K.E.; Hussain, S.M.; Johnson, G.R. Lysozyme catalyzes the formation of antimicrobial silver nanoparticles. *ACS Nano* **2009**, *3*, 984–994. [CrossRef]
22. Shrivastava, S.; Bera, T.; Singh, S.K.; Singh, G.; Ramachandrarao, P.; Dash, D. Characterization of antiplatelet properties of silver nanoparticles. *ACS Nano* **2009**, *3*, 1357–1364. [CrossRef]
23. Chauhan, G.; Madou, M.J.; Kalra, S.; Chopra, V.; Ghosh, D.; Martinez-Chapa, S.O. Nanotechnology for COVID-19: Therapeutics and vaccine research. *ACS Nano* **2020**, *14*, 7760–7782. [CrossRef]
24. Laloy, J.; Minet, V.; Alpan, L.; Mullier, F.; Beken, S.; Toussaint, O.; Lucas, S.; Dogné, J.M. Impact of silver nanoparticles on haemolysis, platelet function and coagulation. *Nanobiomedicine* **2014**, *1*, 4. [CrossRef]
25. Neun, B.W.; Ilinskaya, A.N.; Dobrovolskaia, M.A. Updated method for in vitro analysis of nanoparticle hemolytic properties. In *Characterization of Nanoparticles Intended for Drug Delivery*; McNeil, S.E., Ed.; Methods in Molecular Biology; Humana Press: New York, NY, USA, 2018; Volume 1682, pp. 91–102. [CrossRef]
26. Anandalakshmi, K.; Venugobal, J.; Ramasamy, V. Characterization of silver nanoparticles by green synthesis method using *Pedalium murex* leaf extract and their antibacterial activity. *Appl. Nanosci.* **2016**, *6*, 399–408. [CrossRef]
27. Jang, M.-H.; Lee, S.; Hwang, Y.S. Characterization of silver nanoparticles under environmentally relevant conditions using asymmetrical flow field-flow fractionation (AF4). *PLoS ONE* **2015**, *10*, e0143149. [CrossRef]
28. Chen, S.; Diekmann, H.; Janz, D.; Polle, A. Quantitative x-ray elemental imaging in plant materials at the subcellular level with a transmission electron microscope: Applications and limitations. *Materials* **2014**, *7*, 3160–3175. [CrossRef]
29. Annamalai, J.; Nallamuthu, T. Green synthesis of silver nanoparticles: Characterization and determination of antibacterial potency. *Appl. Nanosci.* **2016**, *6*, 259–265. [CrossRef]
30. Majeed, S.; Khanday, M. Green synthesis of silver nanoparticles using bark extract of Salix Alba and its antimicrobial effect against bacteria isolated from dental plaque. *Orient. J. Chem.* **2016**, *32*, 1611–1618. [CrossRef]
31. Amaliyah, S.; Sabarudin, A.; Masruri, M.; Sumitro, S.B. Characterization and antibacterial application of biosynthesized silver nanoparticles using *Piper retrofractum* Vahl fruit extract as bioreductor. *J. Appl. Pharm. Sci.* **2022**, *12*, 103–114. [CrossRef]

32. Clinical and Laboratory Standards Institute (CLSI). *Performance Standards for Antimicrobial Susceptibility Testing*, 32nd ed.; CLSI Suplement M100; Clinical and Laboratory Standards Institute: Malvern, PA, USA, 2022.
33. Krishnaraj, R.N.; Berchmans, S. In vitro antiplatelet activity of silver nanoparticles synthesized using the microorganism *Gluconobacter roseus*: An AFM-based study. *RSC Adv.* **2013**, *3*, 8953–8959. [CrossRef]
34. Mustard, J.F.; Perry, D.W.; Ardlie, N.G.; Packham, M.A. Preparation of suspensions of washed platelets from humans. *Br. J. Haematol.* **1972**, *22*, 193–204. [CrossRef]
35. Jiang, H.S.; Zhang, Y.; Lu, Z.W.; Lebrun, R.; Gontero, B.; Li, W. Interaction between silver nanoparticles and two dehydrogenases: Role of thiol groups. *Small* **2019**, *15*, 1900860. [CrossRef]
36. Thapa, R.; Bhagat, C.; Shrestha, P.; Awal, S.; Dudhagara, P. Enzyme-mediated formulation of stable elliptical silver nanoparti-cles tested against clinical pathogens and MDR bacteria and development of antimicrobial surgical thread. *Ann. Clin. Microbiol. Antimicrob.* **2017**, *16*, 39. [CrossRef]
37. Khalil, M.M.; Ismail, E.H.; El-Baghdady, K.Z.; Mohamed, D. Green synthesis of silver nanoparticles using olive leaf extract and its antibacterial activity. *Arab. J. Chem.* **2014**, *7*, 1131–1139. [CrossRef]
38. Amin, M.; Anwar, F.; Janjua, M.R.S.A.; Iqbal, M.A.; Rashid, U. Green synthesis of silver nanoparticles through reduction with *Solanum xanthocarpum* L. berry extract: Characterization, antimicrobial and urease inhibitory activities against *Helicobacter pylori*. *Int. J. Mol. Sci.* **2012**, *13*, 9923–9941. [CrossRef]
39. Raju, D.; Mendapara, R.; Mehta, U.J. Protein mediated synthesis of Au–Ag bimetallic nanoparticles. *Mater. Lett.* **2014**, *124*, 271–274. [CrossRef]
40. Das, S.; Langbang, L.; Haque, M.; Belwal, V.K.; Aguan, K.; Roy, A.S. Biocompatible silver nanoparticles: An investigation into their protein binding efficacies, anti-bacterial effects and cell cytotoxicity studies. *J. Pharm. Anal.* **2021**, *11*, 422–434. [CrossRef] [PubMed]
41. Kumar, U.; Ranjan, A.K.; Sharan, C.; Hardikar, A.A.; Pundle, A.; Poddar, P. Green approach towards size controlled synthesis of biocompatible antibacterial metal nanoparticles in aqueous phase using lysozyme. *Curr. Nanosci.* **2012**, *8*, 130–140. [CrossRef]
42. Wang, G.; Hou, H.; Wang, S.; Yan, C.; Liu, Y. Exploring the interaction of silver nanoparticles with lysozyme: Binding behaviors and kinetics. *Colloids Surf. B Biointerfaces* **2017**, *157*, 138–145. [CrossRef]
43. Yakovlev, A.V.; Golubeva, O.Y. Synthesis optimisation of lysozyme monolayer-coated silver nanoparticles in aqueous solution. *J. Nanomater.* **2014**, *2014*, 460605. [CrossRef]
44. Singh, H.; Du, J.; Singh, P.; Yi, T.H. Extracellular synthesis of silver nanoparticles by *Pseudomonas* sp. THG-LS1. 4 and their antimicrobial application. *J. Pharm. Anal.* **2018**, *8*, 258–264. [CrossRef] [PubMed]
45. Danaei, M.; Dehghankhold, M.; Ataei, S.; Hasanzadeh Davarani, F.; Javanmard, R.; Dokhani, A.; Khorasani, S.; Mozafari, M.R. Impact of particle size and polydispersity index on the clinical applications of lipidic nanocarrier systems. *Pharmaceutics* **2018**, *10*, 57. [CrossRef] [PubMed]
46. Devi, L.S.; Joshi, S.R. Ultrastructures of silver nanoparticles biosynthesized using endophytic fungi. *J. Microsc. Ultrastruct.* **2015**, *3*, 29–37. [CrossRef]
47. Vanaja, M.; Annadurai, G. *Coleus aromaticus* leaf extract mediated synthesis of silver nanoparticles and its bactericidal activity. *Appl. Nanosci.* **2013**, *3*, 217–223. [CrossRef]
48. Liu, Y.; Guo, R. Synthesis of protein–gold nanoparticle hybrid and gold nanoplates in protein aggregates. *Mater. Chem. Phys.* **2011**, *126*, 619–627. [CrossRef]
49. Dakal, T.C.; Kumar, A.; Majumdar, R.S.; Yadav, V. Mechanistic basis of antimicrobial actions of silver nanoparticles. *Front. Microbiol.* **2016**, *7*, 1831. [CrossRef]
50. Cheng, G.; Dai, M.; Ahmed, S.; Hao, H.; Wang, X.; Yuan, Z. Antimicrobial drugs in fighting against antimicrobial resistance. *Front. Microbiol.* **2016**, *7*, 470. [CrossRef]
51. Ghodake, G.; Kim, M.; Sung, J.-S.; Shinde, S.; Yang, J.; Hwang, K.; Kim, D.Y. Extracellular synthesis and characterization of silver nanoparticles—antibacterial activity against multidrug-resistant bacterial strains. *Nanomaterials* **2020**, *10*, 360. [CrossRef]
52. Sondi, I.; Salopek-Sondi, B. Silver nanoparticles as antimicrobial agent: A case study on *E. coli* as a model for Gram-negative bacteria. *J. Colloid Interface Sci.* **2004**, *275*, 177–182. [CrossRef]
53. Wu, D.; Fan, W.; Kishen, A.; Gutmann, J.L.; Fan, B. Evaluation of the antibacterial efficacy of silver nanoparticles against *Enterococcus faecalis* biofilm. *J. Endod.* **2014**, *40*, 285–290. [CrossRef] [PubMed]
54. Avalos, A.; Haza, A.I.; Mateo, D.; Morales, P. Cytotoxicity and ROS production of manufactured silver nanoparticles of different sizes in hepatoma and leukemia cells. *J. Appl. Toxicol.* **2014**, *34*, 413–423. [CrossRef] [PubMed]
55. Lee, B.; Lee, M.J.; Yun, S.J.; Kim, K.; Choi, I.H.; Park, S. Silver nanoparticles induce reactive oxygen species-mediated cell cycle delay and synergistic cytotoxicity with 3-bromopyruvate in *Candida albicans*, but not in *Saccharomyces cerevisiae*. *Int. J. Nanomed.* **2019**, *14*, 4801–4816. [CrossRef] [PubMed]
56. Espinosa-Cristóbal, L.F.; Martínez-Castañón, G.A.; Loyola-Rodríguez, J.P.; Niño-Martínez, N.; Ruiz, F.; Zavala-Alonso NVLara, R.H.; Reyes-López, S.Y. Bovine serum albumin and chitosan coated silver nanoparticles and its antimicrobial activity against oral and nonoral bacteria. *J. Nanomater.* **2015**, *2015*, 420853. [CrossRef]
57. Chen, L.Q.; Fang, L.; Ling, J.; Ding, C.Z.; Kang, B.; Huang, C.Z. Nanotoxicity of silver nanoparticles to red blood cells: Size dependent adsorption, uptake, and hemolytic activity. *Chem. Res. Toxicol.* **2015**, *28*, 501–509. [CrossRef]

58. Kwon, T.; Woo, H.J.; Kim, Y.H.; Lee, H.J.; Park, K.H.; Park, S.; Youn, B. Optimizing hemocompatibility of surfactant-coated silver nanoparticles in human erythrocytes. *J. Nanosci. Nanotechnol.* **2012**, *12*, 6168–6175. [CrossRef]
59. Ragaseema, V.M.; Unnikrishnan, S.; Krishnan, V.K.; Krishnan, L.K. The antithrombotic and antimicrobial properties of PEG-protected silver nanoparticle coated surfaces. *Biomaterials* **2012**, *33*, 3083–3092. [CrossRef]
60. Deb, S.; Raja, S.O.; Dasgupta, A.K.; Sarkar, R.; Chattopadhyay, A.P.; Chaudhuri, U.; Guha, P.; Sardar, P. Surface tunability of nanoparticles in modulating platelet functions. *Blood Cells Mol. Dis.* **2012**, *48*, 36–44. [CrossRef]
61. Asghar, M.A.; Yousuf, R.I.; Shoaib, M.H.; Asghar, M.A. Antibacterial, anticoagulant and cytotoxic evaluation of biocompatible nanocomposite of chitosan loaded green synthesized bioinspired silver nanoparticles. *Int. J. Biol. Macromol.* **2020**, *160*, 934–943. [CrossRef]
62. Ernest, V.; Gajalakshmi, S.; Mukherjee, A.; Chandrasekaran, N. Enhanced activity of lysozyme-AgNP conjugate with synergic antibacterial effect without damaging the catalytic site of lysozyme. *Artif. Cells Nanomed. Biotechnol.* **2014**, *42*, 336–343. [CrossRef]